Structural, optical and dielectric properties of (AZT) aluminum doped zinc titanate nano-composites

Y. Srinivas[a], N. V. K. Prasad[a,*], U. Naresh[b], D. B. Basha[c]
[a]*Department of Physics, GSS, GITAM Deemed to be University, Bangalore-562163, India*
[b]*Dept. of Physics, PVKK Institute of Technology, Anantapur-515001, India*
[c]*College of Computer and Information Sciences, Majmaah University, Al'Majmaah, K.S.A-11952*

Aluminum-doped Zinc Titanate (AZT) $Al_xZn_{1-x}TiO_3$ (for x= 0.20,0.40,0.60,0.80) nano-particles are synthesized through low temperature hydrothermal method and their physical properties such as structure, surface, energy gap and dielectric characteristics were investigated using X-ray diffraction (XRD), Field Emission Scanning Electron Microscopy (FESEM), Transmission Electron Microscopy (TEM), UV-visible spectroscopy and impedance analysis. XRD analysis indicated structural transformation of tetragonal phase for samples of x = 0.20 to 0.60 and some secondary phases for x=0.80. It was found that lattice constants of the sample decrease with increasing aluminium content. The morphology of nano-composites, as evidenced by FESEM and TEM imaging, displayed the formation of nano-spheres and nano-rods. The impedance and dielectric modulus analysis for the current samples revealed their dielectric behaviour, microstructure and conduction procedure. However negative dielectric property was seen in nano-composite with x=0.60. All samples with x ranging between 0.2 to 0.8 displayed high ac-electrical conductivity at 1 MHz frequency. These samples are well suitable for charge storage capacitors and as perfect absorbers.

(Received April 15, 2024; Accepted July 15, 2024)

Keywords: AZT, XRD, SEM, TEM, FESEM

1. Introduction

Nanomaterials have a critical role in improvement of energy storage devices and capacitors. They have unique properties that enhance performance and efficiency. For example, nanomaterials can increase surface area, which is particularly beneficial in capacitors, as it allows for more charge storage. The advancements in energy storage, conversion, and shielding technologies have been fascinating. Capacitors, batteries, microwave absorbers, and fuel cells play crucial role in meeting the ever-growing global energy demands. Each device has unique strength and applications, contributing to a more sustainable and efficient energy landscape. It's essential to search for materials that can boost the efficiency of these devices. The continuous advancements in efficiency, energy density, and lifespan are crucial for the development of more reliable and sustainable energy solutions. Carbon nanotubes (CNTs) and graphene are popular choices due to their excellent electrical conductivity and high surface area. They are used to improve the electrodes in supercapacitors, which enable faster charge and discharge rates. Nanostructured metal oxides, such as titanium dioxide and manganese oxide, are also being explored for their potential in lithium-ion batteries. Their nanoscale features enhance ion diffusion and storage capacity [1]. Metal oxides, such as titanium dioxide and manganese oxide are being studied for their potential use in lithium-ion batteries. These oxides have nanoscale features that can improve ion diffusion and storage capacity [2]. Capacitors are energy-storing devices that typically boast high power density but low energy density. However, the development of super capacitors has yielded promising results, as they have proven to be highly efficient with moderate power and

* Corresponding author: vnarasip@gitam.edu
https://doi.org/10.15251/JOR.2024.204.493

energy, while also exhibiting impressive longevity when compared to other energy storage devices [3]. Generally, super capacitors come in two main varieties: Electric double-layer capacitors (EDLCs) and pseudo-capacitors and each type boasts its own set of advantages. The EDLCs excel at providing high power density and fast charge/discharge cycles. Both EDLCs and pseudo-capacitors store electrical energy through physical adsorption of charge storage ions at the interface between the electrode and the electrolyte. Nevertheless, pseudo capacitors are particularly effective at controlling fast surface redox reactions at this interface, which results in a higher specific capacitance, which makes them suitable for scenarios where a more sustained release of energy is needed. The interaction between these different types of supercapacitors allows us to tailor energy storage solutions to specific requirements. It's this versatility that keeps pushing the boundaries by achieving a combination of different types of supercapacitors allowing us to create energy storage solutions that are customized to meet specific requirements. This versatile approach enables us to continuously push the boundaries of energy storage technology. Moreover, when we combine EDLC and Pseudo supercapacitors, we can improve the cell voltage too [4-5]. Combining different types of supercapacitors allows us to create energy storage solutions that can be tailored to meet specific requirements. The combination of EDLC and Pseudo supercapacitors in an asymmetric-based hybrid supercapacitor configuration has been observed to improve cell voltage. This approach has the potential to enhance energy storage technology by pushing the boundaries of current capabilities.

Utilizing nanoparticles can significantly enhance environmental sustainability, energy efficiency, and technological innovation, making them an invaluable resource for various industries. The high surface area of these nanoparticles is advantageous for catalytic reactions and adsorption processes. Titanate nanoparticles have been extensively studied for environmental remediation, particularly in removing heavy metals from water. Their ability to selectively bind to certain ions makes them effective in purification processes [7]. Titanate nanoparticles possess unique structural and physical properties that can significantly enhance the performance of batteries and capacitors. As a result, they have been researched for their potential applications in energy storage and environmental uses. Of particular interest to researchers is their potential use in lithium-ion batteries, which could lead to increased energy density and higher overall efficiency. Furthermore, titanate nanoparticles have shown promise in medical applications. They can be functionalized for drug delivery systems, allowing for targeted and controlled release of pharmaceuticals.

Perovskites are materials with the ABO3 structure, containing divalent/trivalent cations A and B. These compounds have unique electronic, magnetic, and optical properties that can be tuned by modifying their composition and structure. Their versatility makes them promise to advance various technological applications. The Zinc titanate (ZTO) or $ZnTiO_3$ has gained significant interest because of its unique physical and chemical properties, high refractive index, and wide bandgap. Within the crystal structure of perovskite $ZnTiO_3$, there are occupied Zn^{2+} and Ti^{4+} sites that makeup 2/3 of the octahedral void and rhombohedral. The remaining 1/3 of the void is available for use as a pigment, catalyst, or phosphor matrix. This material has luminescence properties that can be adjusted by doping Rare Earth and Transition Elements in the $ZnTiO_3$ matrix. This makes it an ideal choice for efficient luminescence applications due to its tuneable energy levels and bandgap.

Zinc Titanate is a versatile material widely used in LED devices, and solar cells for solar spectrum conversion, and bioimaging. Its unique properties make it ideal for enhancing the quality of medical imaging and diagnosis. Zinc Titanate is also used in electronic ceramics, catalysts, and optical fibres. However, the research on its application in temperature sensing is still relatively limited. Hence, studying this aspect could be a worthwhile direction to explore. Zinc-based electrodes have shown great potential for use in supercapacitors. However, their practical application has been hindered by poor repeatability and low-rate capability during cycling. Fortunately, researchers have found a solution by incorporating compounds made of transition and rare earth elements along with zinc oxide as electrode materials. This ingenious combination of Faradaic capacitance and double-layer capacitance leads to a significantly larger surface area, resulting in improved capacitance and cycling stability [11]. These types of studies are significant in the field of energy storage and could lead to the creation of more efficient and dependable

supercapacitors. In the development of Zinc grounded electrodes as a probable material for supercapacitors, certain challenges need to be addressed before its practical application. However, by using composites made up of transition metals and zinc oxide as electrode materials, electrochemical capacitors can overcome several serious limitations. The fusion of Faradaic capacitance from metal oxide and double-layer capacitance from composites results in a substantial increase in surface area, leading to improved capacitance and cycling stability. These discoveries bear significant implications in the energy storage domain, offering potential advancements in the efficiency and dependability of supercapacitors [11]. Such insights pave the way for the development of supercapacitors with heightened performance attributes, with broad applicability across various sectors requiring efficient energy storage solutions.

The following reports are motivated to proceed with the hydrothermal synthesis of $ZnTiO_3$ for use in supercapacitors. Prior research in the literature suggests that Titanium-based ternary metal oxides stand out for lithium-ion batteries as highly promising anode materials, primarily owing to their advantageous safety characteristics. These materials have excellent chemical and electrical properties, high transfer capacity, adjustable conductivity, and multiple redox reactions. Some examples of such materials include Zn_2TiO_4, $ZnTiO_3$, and $Zn_2Ti_3O_8$. Among these, $ZnTiO_3$ has a higher theoretical capacity and is also more cost-effective than other Zn, Ti-based oxides containing lithium [12]. Bakr et.al [13] synthesised Al, Fe, and Cu-doped $ZnTiO_3$ through the sol-gel process and studied the optical and dielectric properties, the results revealed that the energy band gap is 3.4eV and the dielectric constant of $ZnTiO_3$ raised by doping the Aluminium. Nahrawy et.al [14] studied the effect of Al_2O_3 on $ZnTiO_3$ material's structural and morphological and dialectic properties. The average crystallite of the Al_2O_3 / $ZnTiO_3$ is decreased as increasing the Al, the dielectric loss and tanδ less than one and the dielectric loss decreases as increasing the Al concentration. Hemalatha Reddy et.al [15] prepared gold deposited ZnTiO3 nanostructures for the improvement of photocatalytic activities, the studies provided the information that the $ZnTiO_3$ energy gap decreased by coating of gold by precipitation method. Bhardwaj et.al [16] fabricated ZnTiO3 nanoparticles through the solid-state synthesis method for battery electrode fabrication and electrochemical analysis carried out, the result revealed the zinc process titanate may considered a promising material for the Zinc Air batteries with a excellent cyclic abilities. Mansour et.al [17] prepared SiO_2-$ZnTiO_3$ nanostructure via sol-gel process and analysed dielectric, optical properties and found that the energy lies about 3eV dielectric constant and loss in order of 8 and 0.12 so this material suitable for the microwave absorbers. Siragam et.al [18] prepared zinc aluminate and zinc aluminate titanate using the sol-gel preparation technique, and the average diameter and particle size obtained in the order of 10nm to 20nm nanomaterials. Interestingly, regarding the prototype antenna application the calculation of voltage standing wave ratio (VSWR) found as the return loss and found as negative the reason noted as increased dielectric permittivity, and reduction of tangent loss.The titanate and its composites were synthesised through different preparation techniques such as sol-gel, co-precipitation, auto-combustion, solid state method and hydrothermal. Above all, the hydrothermal method is an appropriate and considerable technique to make nanoparticles and composites in the production of nanoparticles and composites at a lower temperature [19]. In the present study, aluminum-doped zinc titanate nanoparticles are synthesized through the hydrothermal method and characterization was carried out for the analysis of structural, morphological, energy gap estimation and dielectical properties.

2. Materials and methods

Hydrothermal method was chosen for the synthesis of aluminium zinc titanate $Al_xZn_{1-x}TiO_3$ (x= 0.2,0.4,0.6,0.8) (AZT) nano-composites. All the chemicals were purchased from Sigma-Aldrich co. ltd given by $Zn(NO_3)_2.6H_2O$(99.9 % purity), $(NO_3)_3.9H_2O$(99.8 % purity and TiO_2(99.9 % purity). In order to prepare the nano-composite solution, the precursors were mixed in distilled water as per the required stoichiometric ratio and continuously stirred at a rate of 500 rpm for half an hour under room temperature. This solution was subjected to heating at 150°C for 8 hours using a stainless steel autoclave. Once the reaction is completed, the nano-composite

solution was cooled, extracted and washed multiple times. Finally, the solution was dried for 2 to 3 hours at 100°C. The same procedure was followed for all samples of x = 0.20 – 0.80 . Later, the prepared compound was made as fine powder and these samples were utilised for characterisation using XRD, TEM, FESEM, UV-visible spectrometer and LCR meter.

3. Results and discussion

3.1. XRD analysis

XRD pattern of AZT nano-particles (x = 0.20 - 0.80) was examined and found to have a well-crystalline structure. The intensity of samples with x = 0.20, 0.40 and 0.60 was maximum for $2\theta = 25.46^0$, while for samples with =0.80 intensity was peaked at $2\theta = 25.46^0$ and 31.42^0. Figure.1 confirmed phase transformation from cubic to tetragonal for all current samples. The diffraction positions for samples with x ranging from 0.2 to 0.8 were compared to the standard JCPDS card 84-4921. It was observed that the sample with x = 0.8 displayed some secondary phases showing reflection planes similar to those of JCPDS: 87-1781.

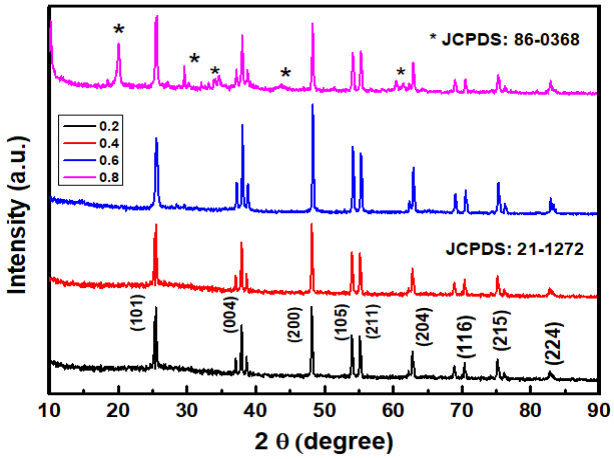

Fig. 1. XRD spectra of AZT nano-particles.

Table 1:Observed Crystal Parameters for various compositions of AZT nano-particles

x	0.20	0.40	0.60	0.80
a =b (nm)	3.210	4.100	4.200	4.700
c (nm)	8.900	9.000	9.200	9.300
D (nm)	59.5	58.4	51.5	50.2
V (nm)	91.70	151.29	162.28	205.43
ρt (g/cm^3)	3.670	2.359	2.320	1.928
ρe (g/cm^3)	3.193	1.934	1.763	1.195
Porosity (P)	0.13	0.18	0.24	0.38
S (m^2/g)	27.70	43.84	50.70	62.22

Hence the samples with x = 0.20, 0.40 and 0.60 obtained tetragonal structure and for x =0.80 the sample consist of cubic minor secondary phases related to $Zn_2Ti_3O_8$. It is commonly believed that the formation of a secondary phase in a composite system is due to the differences in the ionic radii, the ionic radii of Al^{+3}, Ti^{+4}, and Zn^{+2} are 0.039 nm, 0.068 nm, and 0.060 nm, respectively. Titanium cations have a larger ionic radius than the other cations. The well-known Scherrer relation is used to find the average crystallite diameter that is [20]:

$$D = \frac{0.90\lambda}{\beta\cos\theta} \quad (1)$$

where 'λ'=0.15418 nm represent X-ray wavelength,'θ'= diffraction angle and 'β' represent full-width half maxima(FWHM).

The value of 'D' for x=0.20 to 0.80 is found to decrease from 59 to 50 nm, respectively. This nature exists due to the fact that an increase in FWHM from 0.110 radians to 0.153 radians for x = 0.20 to 0.80 since FWHM and D are inversely proportional. The lattice constants are determined using the equation(2):

$$1/d^2 = (h^2+k^2)/a^2 + l^2/c \quad (2)$$

where 'd' represent inter planar space, h, k, l represent Miller indices and a & c are the lattice constants for tetragonal a=b not equal to c.

Table.1 displays the results which indicate that all lattice parameters increase with increase in concentration of aluminium. The unit cell volume (V) was found to be 91.7064, 151.29, 162.28 and 205.43 in units of $Å^3$ for x = 0.2, 0.4, 0.6, and 0.8 respectively. X-ray density was calculated from the equation (3):

$$\rho x \left(\frac{g}{c.c}\right) = \frac{Z*Moliculer\ weight}{N*V} \quad (3)$$

where Z=4 for tetragonal and Z=1 for cubic representing total number of atoms and 'N' the Avogadro's number ($6.023x10^{23}$). As mentioned earlier Table.1 displayed the calculated values which are increasing with aluminium concentration. The rate of increment for the X-ray density is expected because the volume and molecular weight are in increasing manner. Furthermore, upon conducting a detailed analysis, it was observed that the sample with x = 0.2 had an exceptionally low specific surface area (S). However, for the samples ranging from x = 0.4 to 0.8, the specific surface area was observed to vary between 149.7 to 248.3 m2/g. This variation in the specific surface area of samples with increasing values of x indicates the improvement of the electrical properties of the material. It is important to note that a higher value of S indicates an increased surface area per unit mass of the material, which can lead to better electrical conductivity.

3.2. FESEM and TEM analysis

Field emission scanning electron microscopy (FESEM) and Transmission electron microscopy (TEM) are used to analyse the surface morphology of AZT (X= 0.2, 0.4, 0.6 and 0.8) nano-composites.

The FESEM pictures of the 200 nm magnification are shown in Figure 2. It is clear from the figure that the morphology changes from spheres to plates with increasing aluminium concentration. Images of 0.2 concentration reflect the agglomerated cluster of spheres with an average grain size of 112.7nm for x=0.2. In the figure for x=0.4, we can observe the variation in morphology from spheres to fibres, the average grain size also increased to 141 nm [21]. Further, for aluminium concentration x=0.6 variation in morphology is observed with an average grain size of 201nm. For x = 0.8, morphology changes appear in the form of big size plates with inclusion of large number of spheres and huge agglomeration between the plates. Hence, it was concluded that an increase in aluminium content within the composite system resulted in a change of morphology, with larger numbers of spheres transforming into smaller nanofibers, and ultimately into larger plate-like structures. FESEM studies are in good coincidence with TEM nano-graphs as shown in Figure 3. We noticed that at x = 0.4 very small fiber-like morphology was initiated with variation towards plate like structures in FESEM studies and TEM micrographs. The XRD spectra was in good agreement for this variation in morphology because the XRD spectra of 0.6 have limited number of secondary phases then 0.8 spectra.

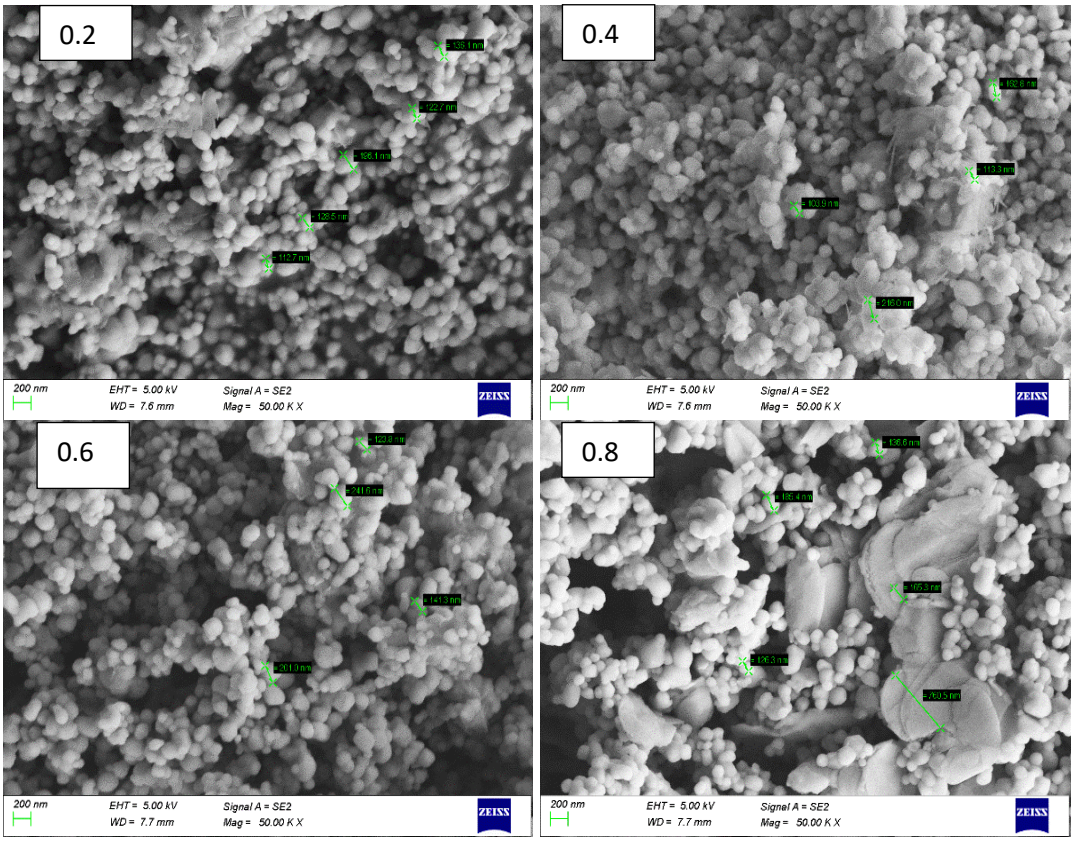

Fig. 2. FESEM images of AZT nanoparticles.

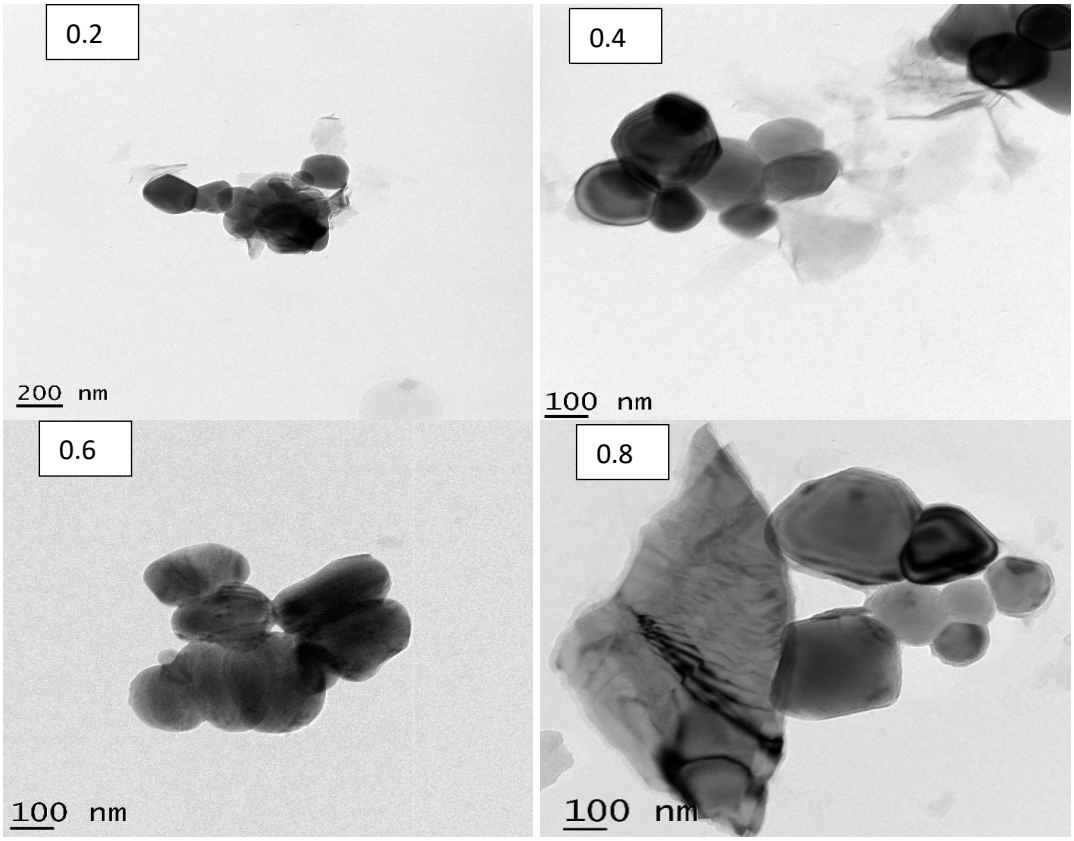

Fig. 3. TEM nano-graphs of AZT nanoparticles

3.3. UV-visible spectroscopy

The band gaps of AZT samples for x (0.2, 0.4, 0.6, and 0.8) were investigated using UV-visible spectroscopy. Figure.4 shows the results obtained. To determine the energy band gap of the synthesized samples, Tauc plot analysis was carried out, using the known relationship for energy band gap given by equation (4).

$$\alpha h\upsilon = A\,(h\upsilon - E_g)^2 \tag{4}$$

The band gap was appraised using α (absorption coefficient), h (Planck's constant), υ (frequency of incident radiation) and E_g (band gap energy).

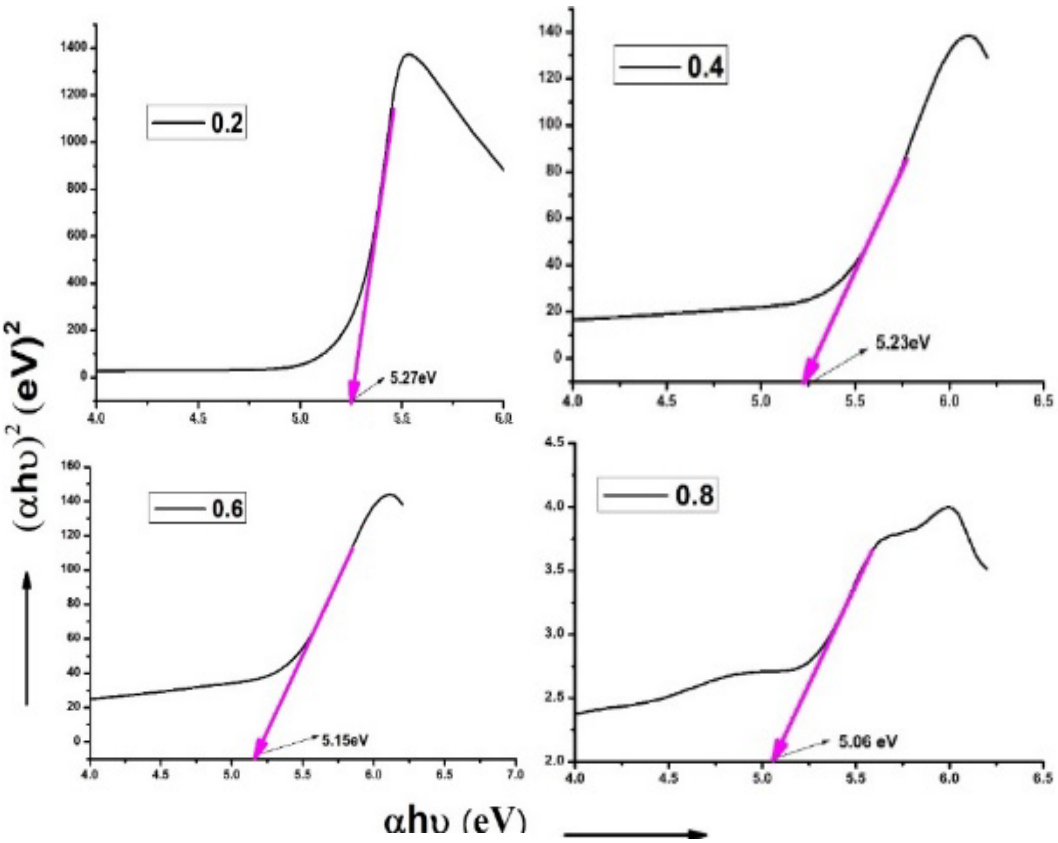

Fig. 4. Energy band gap estimation of AZT nanoparticles.

To determine the energy bandgap, a tangent line is drawn to the straight, upright part of the curves and then extrapolated to the x-axis. This technique is commonly used to calculate the energy gap values in semiconductors. In this experiment, the energy gap values were measured for four different concentrations: 0.2, 0.4, 0.6, and 0.8. The results showed that the energy gap values were 5.27 eV, 5.23 eV, 5.15 eV, and 5.06 eV, respectively. It is worth noting that the energy bandgap is a fundamental property of semiconductors and plays a significant role in their electrical behavior. This type of behavior has also been observed in previous studies and is consistent with the expected behavior of semiconductors.

3.4. Dielectric properties

The researchers analyzed the dielectric properties of the AZT nano-particles at room temperature using an impedance analyser to measure the dielectric loss and dielectric constant between 10 MHz and 50MHz and the analysis was carried out by plotting calculated dielectric constant (ε') and frequency (log ω) as well as dielectric loss (ε") against frequency (log ω).The resultant plots are presented in Figures 5a & 5b.

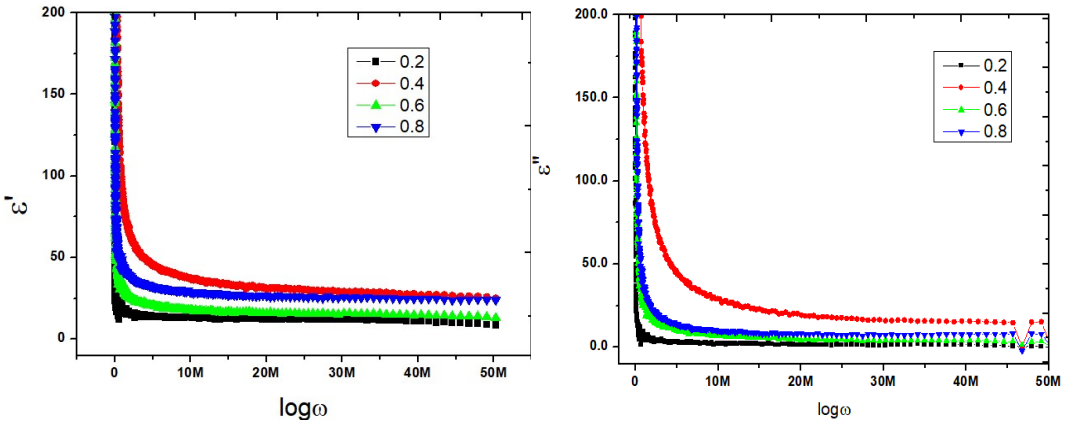

Fig. 5. (a) Frequency dependence dielectric properties of AZT nano-composites; (b) Frequency dependence dielectric properties of AZT nanocomposites.

Figure 5a indicated a significant increase in ε' for samples with x values between 0.2 and 0.8. This behaviour is commonly associated at the interface of grain boundary at low value of logw due to presence of space charge species. Consequently, polarization develop gradually, leading to what is known as Maxwell-Wagner's polarization [23], which is known to cause a rise in the dielectric constant. This plot also indicated an increase in ε' from 3727 to 14166 (x = 0.2 to 0.6) and the value decreased to 5081 in case x = 0.80. Figure 5b displayed an increase in ε" from 566 to 15340 for x = 0.2 to 0.6 while a decrease to 1509 for x = 0.80. At 1 MHz, similar behaviour was seen between 230 to 710 for x = 0.2 – 0.6 samples and decreased to 252 for x=0.80. Except for x = 0.6, similar behaviour was seen for all other samples between 6 to 8 MHz. From the above two plots dielectric relaxation was seen for log ω = 5 to 6.35 for all samples which might be attributed to charge build up at sample interface. It is noteworthy that sample with x=0.60 exhibit negative dielectric characteristics with ε' ~ -58.5 and ε" ~ -417, indicating a switch from positive to negative behaviour at a frequency of 6 MHz. The dielectrics can enhance charge storage capacity when they are placed between two conductive plates to increase the capacitance with positive dielectric constant.However, in some cases, materials can exhibit negative dielectric behaviour, which is a rare property. This behaviour was previously observed in perovskite materials and metamaterials. Nanocomposites, which are not metamaterials, can also exhibit negative dielectric behaviour due to their geometric properties.

When a nano-composite is placed in electric field it leads to negative polarization. This is due to increase in negative dielectric constant and dielectric loss due to charge carriers aligning in opposite directions. This fact is also explained by taking the diamagnetic nature where the material shows negative magnetization by application of a magnetic field. Therefore, in the case of dielectric, the polarization develops opposite to the direction of the applied electric field frequency. This rare property of negative dielectric behaviour can lead to new possibilities for designing and developing advanced materials. Researchers have found that the nanocomposite with an x value of 0.6 performs similarly to other high dielectric constant nanocomposites (x =0.2, 0.4, and 0.8) between 6-8 MHz. These nanocomposites are ideal for applications requiring high-charge storage capacitors. The negative dielectric behaviour was observed for sample with x = 0.6.

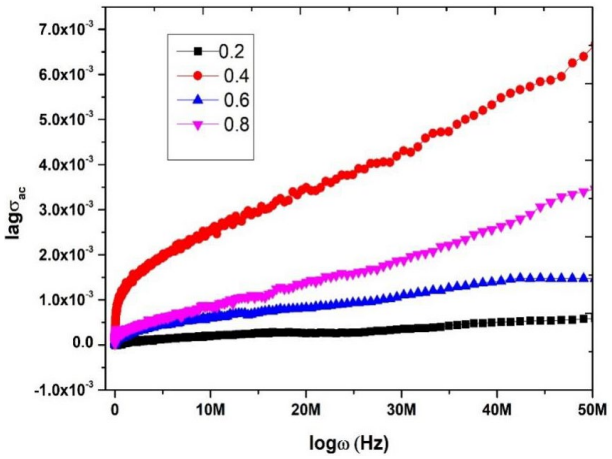

Fig. 6. AC- electrical conductivity versus log ω.

AC electrical conductivity can be calculated using equation(5):

$$\sigma_{ac} = \varepsilon_o \varepsilon'' \omega \tag{5}$$

where 'ε_o'is the permittivity of free space and the other symbols have their conventional definitions. Figure.6 illustrates the correlation between electrical conductivity and frequency. It shows a series of graphs that plot log σ_{ac} against log ω. It was observed that σ_{ac} was very small at low values of log ω and increased significantly as log ω increased. This behaviour was noticed for x = 0.2, 0.4, and 0.8 samples. In the case of the sample with x = 0.6, the ac-electrical conductivity becomes a negative value between 6 to 8 MHz frequency. However, at a frequency of 1 MHz, all nanocomposites exhibited a conductivity ranging from 0.0142 to 0.0976 S/cm, indicating high conductivity at room temperature. The sample with x = 0.6 showed a conductivity of -0.159 S/cm at 6 MHz, which was attributed to its negative dielectric loss.

Figures.7 a & b displays the change in Z' and Z'' with log ω, where Z' represents the real part and Z'' represents the imaginary part of impedance. At low values of log ω, Z' & Z'' are extremely high which is due to space charge drift while it is exactly opposite at high log ω values indicating a decrease in charge species at higher frequencies.

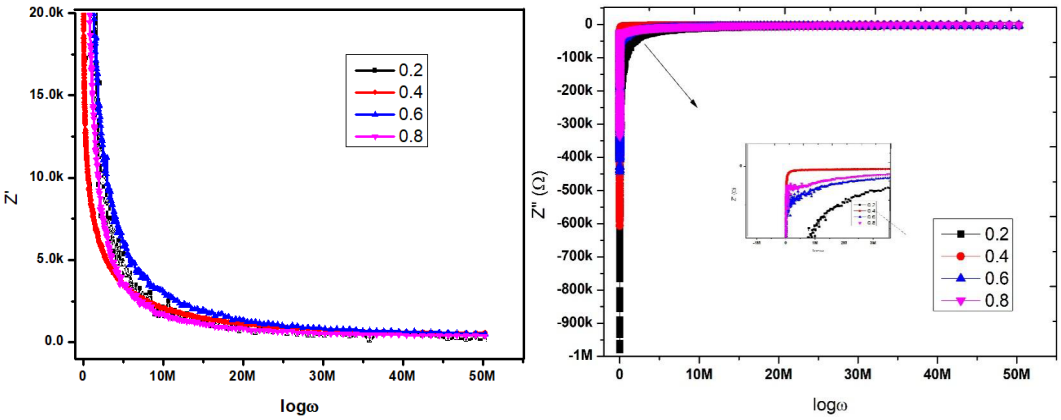

Fig. 7. (a) and (b) Z' and Z'' vs logw plots of AZT nanocomposites.

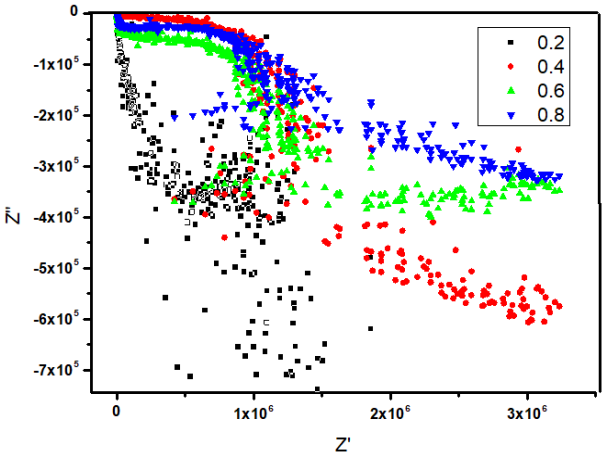

Fig. 8. Cole-Cole plats.

Figure 8 presents the Cole-Cole plots, which provide insights into the electrical characteristics of the samples. Across all samples, the plots reveal the presence of both single and partial semi-circular arcs. These arcs are typically indicative of the impedance response, with partial arcs often attributed to charge carriers that travel long distance within the material. However, an intriguing observation emerges for the sample with x = 0.6: a reverse arc nature is noted at high frequencies. This peculiar behaviour suggests the presence of dielectric properties at those frequencies, hinting at complex interactions within the material's electrical structure.

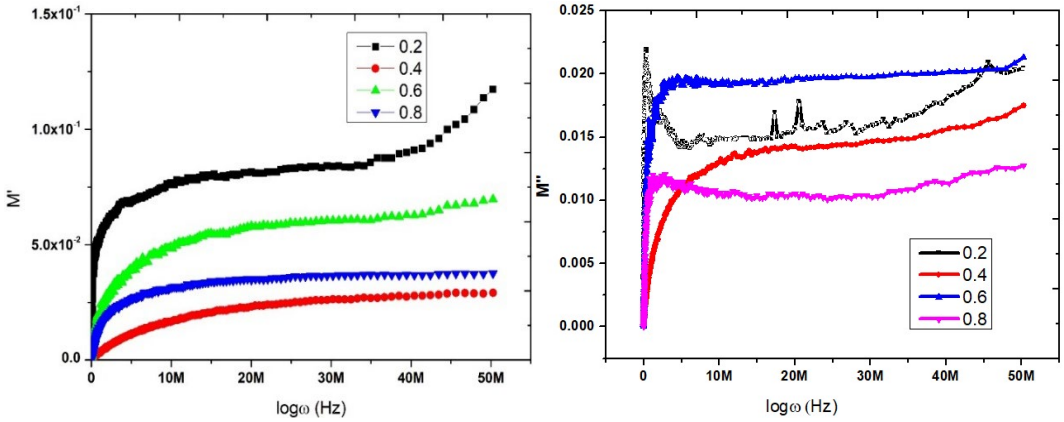

Fig. 9. M'- log ω and M"- log ω plots of AZT nanocomposites.

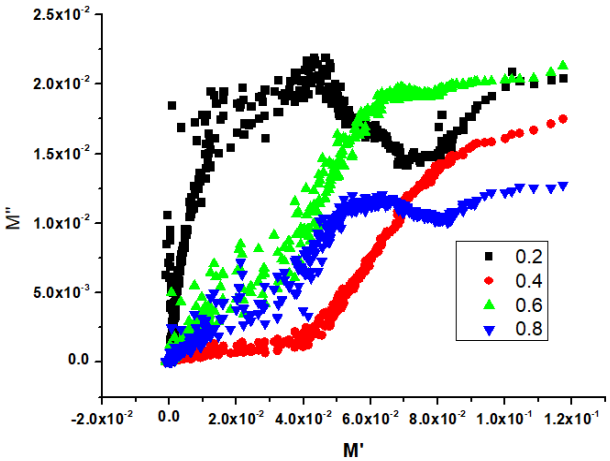

Fig. 10. M' vs M" plots of AZT nanoparticles.

Analysis of dielectric modulus spectrum was done using plots of M' versus log ω, M'' versus log ω (Figure.9) and M' versus M''(Figure.10). Here $M' = \varepsilon'/(\varepsilon'^2+\varepsilon''^2)$ represent real part and $M'' = \varepsilon''/(\varepsilon'^2+\varepsilon''^2$ represent imaginary part. It was observed that M' and M'' are almost zero for very low values of log ω. This behaviour was mainly due to no control on mobility of charges. The charges were unable to return to their original position due to the absence of a restoring force [25]. With increase in frequency, both M' and M'' values escalated rapidly due to short mobility of charges. This demonstrated that nanocomposites with x = 0.20 – 0.80 composition display single or partial semi-circular arcs. However for x = 0.60 sample complete reversal of arc at high frequency was observed, indicating its dielectric behaviour. This kind of nature was observed earlier[26-27].

4. Conclusions

Aluminum doped Zinc Titanates (AZT) were synthesized using low-temperature hydrothermal method. XRD analysis confirmed notable structural transformation from tetragonal phase to cubic phase. For all samples with x values of 0.2, 0.4, 0.6 and 0.8, lattice constants were a = b = 3.774 Å & c = 9.395 Å. Images of TEM and FESEM show formation of nano-spheres to few plates in the morphology. All samples under investigation exhibited high dielectric constant at 1 MHz and high ac-electrical conductivity. Negative dielectric behaviour was seen in composite with x=0.6 between 6 to 8 MHz which is of significance. Impedance and dielectric modulus analysis provided insight into the microstructure and conduction mechanism of charge carriers.

References

[1] B. Venkata Shiva Reddy, K. Srinivas, N. Suresh Kumar, K. Chandra Babu Naidu, (2020) Journal of Materials Science: Materials in Electronics,31,9293; https://doi.org/10.1007/s10854-020-03469-6

[2] A. Mallikarjuna, S. Ramesh, N.S. Kumar, K. Chandra Babu Naidu, K.V. Ratnam, H. Manjunatha, B.P. Rao, (2020), Physica E 122, 114204; https://doi.org/10.1016/j.physe.2020.114204

[3] N. Suresh Kumar, R. Padma Suvarna, K.C. B. Naidu, G. Ranjith Kumar, S. Ramesh, (2021). Ceramics International 44,19408; https://doi.org/10.1016/j.ceramint.2018.07.176

[4] Baba Basha, D. (2018), J Mater Sci: Mater Electron, 32(01),05297; https://doi.org/10.1007/s10854-021-05297-8

[5] Baba Basha, D. (2020), J Mater Sci: Mater Electron, 31,16448; https://doi.org/10.1007/s10854-020-04199-5

[6] E. Veena, A. Mallikarjuna, B. Basha, M. Sekhar, T. Rajender, G. Sujatha, T. Anil Babu, N. V. Krishna Prasad, B. Reddy, (2022), Digest Journal of Nanomaterials and Biostructures, 17(1), 317; https://doi.org/10.15251/DJNB.2022.171.317

[7] T. Su, H. Chen, Z. Wei, M. Hao, X. Wang, Y. Liu, C. Ma, Y. Miao, F. Gao, (2024); Ceramics International, 50(3),317; https://doi.org/10.1016/j.ceramint.2023.11.249

[8] S. Bhaskar Reddy, K. Prasad Rao, M. S. Ramachandra Rao, 2009, J. Alloys Compds. 48(1),692; https://doi.org/10.1016/j.jallcom.2009.03.075

[9] M. Prakash, R. Jeevan Kumar, K. Chandra Babu Naidu, 2020, Mater. Res. Express 7(1), 015037; https://doi.org/10.1088/2053-1591/ab6494

[10] De Abreu Lima, C. D., Dos Santos Sousa, R., Miranda, A. W., Moura, J. V. B., De Sousa Pinheiro, G., Viana, B. C., Lima, I. S., Oliveira, T. M. B. F., Baffa, O., Araujo, J. F. D. F., Luz Lima, C. D, (2023), Solid State Sciences,138,107134; https://doi.org/10.1016/j.solidstatesciences.2023.107134

[11] S. Yang, X. Gao, W. Li, Y. Dai, J. Zhang, X. Zhang, H. Yue, (2023), Journal of Materials Research and Technology,28,1900; https://doi.org/10.1016/j.jmrt.2023.12.059

[12] V. G. Sreeja, P. Hajara, R. Reshmi, E. I. Anila, (2021), Thin Solid Films,722,138580; https://doi.org/10.1016/j.tsf.2021.138580

[13] A. M. Bakr, Ali. B. Abou Hammad, A. R. Wassel, M. Amany, El. Nahrawy, A. M. Mansour, (2021), Int. J.MaterialsEngineering Innovation, 12(2),115; https://doi.org/10.1504/IJMATEI.2021.115604

[14] A. M. E. Nahrawy, A. B. A. Hammad, A. M. Bakr, (2019), Appl. Phys. A, 125(54)2350; https://doi.org/10.1007/s00339-018-2350-6

[15] K. H. Reddy, S. Martha, K. M. Parida, Nanoscale,10.1840(2018); https://doi.org/10.1039/C8NR06158K

[16] Upasana Bhardwaj, Aditi Sharma, H. S. Kushwaha (2023), Mater. Adv., 4, 4197; https://doi.org/10.1039/D3MA00183K

[17] Mansour, Abd el-fattah & Hammad, Ali, Bakr, Ahmed, El Nahrawy, Amany M., Zinc Titanate Wide Bandgap Semiconductor Nano crystallites: Synthesis and Characterization. Silicon. 14,11715; https://doi.org/10.1007/s12633-022-01886-2

[18] S. Srilali, D. S. Raghvendra, P. Lakshman, G. Satheesh, ACS Omega,7(27) (2022); https://doi.org/10.1021/acsomega.2c01671

[19] K. Chandra Babu Naidu. S. Sarmash, M. Maddaiah, P. Reddy, D. Rani, T. Subbarao, (2016), Journal of the Australian Ceramic Society, 52,95.

[20] B. V. S. Reddy, N. Suresh Kumar, T. Anil Babu, S. Ramesh. K. Srinivas, K. C. B. Naidu, (2021), Journal of Materials Science: Materials in Electronics. 32(01,)6625; https://doi.org/10.1007/s10854-021-06625-8

[21] N. S. Kumar, R. P. Suvarna, K. R. Krishna Reddy, T. Anil Babu, S. Ramesh, B. V. Shiva Reddy, H. Manjunatha, K. C. B.Naidu, (2022), Materials Chemistry and Physics, 278, 125598; https://doi.org/10.1016/j.matchemphys.2021.125598

[22] U. Naresh, R. J. Kumar, K. Chandra Babu Naidu, (2019), Ceramics International,45,7515; https://doi.org/10.1016/j.ceramint.2019.01.044

[23] U. Naresh, R. J. Kumar, K. Chandra Babu Naidu, (2019), Materials Chemistry and Physics, 236,121807; https://doi.org/10.1016/j.matchemphys.2019.121807

[24] U. Naresh, R. Jeevan Kumar, K. C. B. Naidu, (2019), Bio-interface Research in Applied Chemistry 09, 4243; https://doi.org/10.33263/BRIAC95.243247

[25] T. F. Khan, U. Naresh, T. R. Ramprasad, R. Jeevan Kumar, (2021), Journal of Superconductivity and Novel Magnetism, 34,797; https://doi.org/10.1007/s10948-020-05788-5

[26] N. Suresh Kumar, R. P. Suvarna, K. C. B. Naidu, (2017), Journal of Materials Science Materials in Electronics, 29, 4378; https://doi.org/10.1007/s10854-017-8429-6

[27] D. Kothandan, R. J. Kumar, K. C. B. Naidu, (2017), Journal of Asian Ceramic Societies, 06(01),01; https://doi.org/10.1080/21870764.2018.1439607